JOURNAL OF AIRCRAFT
Vol. 43, No. 3, May–June 2006

Bifurcation Analysis of Airfoil in Subsonic Flow with Coupled Cubic Restoring Forces

B. H. K. Lee*
National Research Council, Ottawa, Ontario K1A 0R6, Canada
and
L. Liu†
University of Texas Pan American, Edinburg, Texas 78541

The effects of coupled nonlinearities in the pitch and plunge degrees of freedom of an airfoil placed in a subsonic airflow are studied using a numerical time-marching scheme. The initial conditions are fixed, and the airfoil parameters are adopted from a previous study where primary and secondary Hopf bifurcations and modulated oscillations in a subcritical Hopf bifurcation were observed. The investigation is first carried out for fixed spring stiffness in the pitch degree of freedom while the plunge spring constant is varied. The second example fixes the plunge spring constant and varies the pitch spring stiffness. Both weak and strong restoring forces are considered. It is shown that coupled nonlinearities can generate a variety of motions and that chaotic behavior is possible in a narrow window of the bifurcation parameter.

Nomenclature

a_h	=	nondimensional distance from airfoil midchord to elastic axis
b	=	airfoil semichord
$C_L(\tau)$, $C_M(\tau)$	=	aerodynamic lift and pitching moment coefficients
c	=	airfoil chord
f	=	nondimensional linear frequency
h	=	plunge displacement
m	=	airfoil mass
r_α	=	radius of gyration about elastic axis
t	=	time
U	=	freestream velocity
U^*	=	nondimensional velocity, $U/b\omega_\alpha$
U_L^*	=	linear flutter speed
$\boldsymbol{X}$	=	eight-dimensional vector variable
x_α	=	nondimensional distance from airfoil elastic axis to center of mass
α	=	pitch angle of airfoil
β	=	cubic coefficient in pitch
γ	=	cubic coefficient in plunge
ε_1, ε_2	=	constants in Wagner's function
ζ_α, ζ_ξ	=	viscous damping ratios in pitch and in plunge
μ	=	airfoil/air mass ratio, $m/\pi\rho b^2$
ξ	=	nondimensional plunge displacement, h/b
τ	=	nondimensional time, Ut/b
$\phi(\tau)$	=	Wagner's function
ψ_1, ψ_2	=	constants in Wagner's function
ω	=	fundamental frequency of motion
ω_ξ, ω_α	=	natural frequencies in plunge and in pitch
$\bar{\omega}$	=	frequency ratio, ω_ξ/ω_α

Received 12 October 2004; revision received 28 October 2005; accepted for publication 1 November 2005.

*Principal Research Officer, Aerodynamics Laboratory, Institute for Aerospace Research. Associate Fellow AIAA.

†Assistant Professor, Department of Mathematics; LipingLiu@utpa.edu. Member AIAA.

Introduction

AIRFOIL motion with cubic restoring forces has been studied as early as the 1950s by Woolston et al.[1] and Shen,[2] and a recent review of this topic can be found in Ref. 3. O'Neil et al.[4] carried out experiments to demonstrate the existence of limit-cycle oscillations in aeroelastic systems with cubic nonlinearities in the pitch degree of freedom and showed favorable comparisons of their results with numerical simulations. Except for the wind-tunnel studies carried out by Hauenstein et al.,[5] where two coupled freeplay nonlinearities were investigated, practically all experimental aeroelastic investigations considered only a single nonlinearity. To the best of the authors' knowledge, experimental studies on the behavior of an airfoil with coupled cubic nonlinearities in the pitch and plunge degrees of freedom have not been reported in the literature, although some simple cases of limit-cycle oscillations were investigated numerically by Alighanbari.[6]

Recently, Lee et al.[7] investigated airfoil motions with a strong cubic nonlinearity in the pitch degree of freedom. Particular emphasis was placed on the occurrence of limit-cycle oscillations and the phenomenon of primary and secondary Hopf bifurcations. A third harmonic balance method was developed to give a frequency–amplitude relation that depends only on airfoil parameters. Whereas the method generally yields accurate results for the amplitude and frequency of the pitch and plunge motions for primary Hopf bifurcations, the secondary bifurcation required the inclusion of a large number of terms in the Fourier series representation of the airfoil motion. The method was later extended by Liu and Dowell,[8] and they considered terms up to 13 harmonics. The algebra becomes so complex that a frequency–amplitude relation similar to that determined by Lee et al.[7] cannot be derived for harmonics higher than the third. Instead, a nonlinear system of algebraic equations has to be solved to predict the secondary bifurcation. The computational procedure is not straightforward and, in fact, is more time consuming than a fourth-order Runge–Kutta numerical scheme commonly used in aeroelastic studies of airfoil motions.[3] This paper provides some interesting observations of the bifurcation phenomenon for an airfoil placed in a subsonic airflow when the magnitude of the cubic restoring forces in the pitch and plunge motions varies from weak to strong. The results are obtained numerically because some of the phenomena reported cannot be predicted from the harmonic balance method[7] or the perturbation–incremental method.[9] The advantage of a numerical time integration scheme is that the effect of initial conditions can be captured, but it has the disadvantage of not being able to predict the unstable branch of a subcritical Hopf bifurcation.

In the study of aeroealstic behavior of an airfoil, it is difficult to make generalizations, especially from numerical simulations, because of the large number of airfoil parameters that we can vary. Different combinations of these parameters can produce quite different airfoil responses. To keep the computations within a reasonable amount of effort, we use the airfoil parameters chosen by Lee et al.[7] In the first case study, the effects of coupled nonlinear pitch and plunge restoring forces are investigated by fixing the constant in the pitch cubic spring and varying the constant in the plunge cubic spring. In the second example, the constant in the plunge cubic spring is fixed while the pitch spring constant is varied.

Equations of Motion of an Airfoil with Cubic Restoring Forces

The symbols used in the analysis of a two-dimensional airfoil motion are given in Fig. 1. The plunge deflection is denoted by h, positive in the downward direction, and α is the pitch angle about the elastic axis, positive nose up. For nonlinear restoring forces, the coupled bending–torsion equations for the airfoil are derived in Ref. 3. In the absence of externally applied forces, they are given in nondimensional form as follows:

$$\xi'' + x_\alpha \alpha'' + 2\zeta_\xi(\bar{\omega}/U^*)\xi' + (\bar{\omega}/U^*)^2 G(\xi) = -(1/\pi\mu)C_L(\tau) \tag{1}$$

$$\left(x_\alpha \Big/ r_\alpha^2\right)\xi'' + \alpha'' + 2(\zeta_\alpha/U^*)\alpha' + (1/U^{*2})M(\alpha) = \left(2\Big/\pi\mu r_\alpha^2\right)C_M(\tau) \tag{2}$$

where $\xi = h/b$ is the nondimensional displacement and the prime denotes differentiation with respect to the nondimensional time $\tau = Ut/b$. The nondimensional velocity is defined as $U^* = U/b\omega_\alpha$. The airfoil/air mass ratio is $\mu = m/\pi\rho b^2$; ζ_α and ζ_ξ are the viscous damping ratios in pitch and plunge, respectively; ω is the frequency; ω_ξ and ω_α are the plunge and pitch natural frequencies, respectively; and $\bar{\omega} = \omega_\xi/\omega_\alpha$. For incompressible flow, Fung[10] gives the following expressions for $C_L(\tau)$ and $C_M(\tau)$:

$$\begin{aligned} C_L(\tau) &= \pi(\xi'' - a_h\alpha'' + \alpha') + 2\pi\left\{\alpha(0) + \xi'(0) + \left[\frac{1}{2} - a_h\right]\alpha'(0)\right\}\phi(\tau) + 2\pi\int_0^\tau \phi(\tau-\sigma)\left[\alpha'(\sigma) + \xi''(\sigma) + \left(\frac{1}{2} - a_h\right)\alpha''(\sigma)\right]\mathrm{d}\sigma \end{aligned} \tag{3}$$

$$\begin{aligned} C_M(\tau) &= \pi\left(\frac{1}{2} + a_h\right)\left\{\alpha(0) + \xi'(0) + \left(\frac{1}{2} - a_h\right)\alpha'(0)\right\}\phi(\tau) + \pi\left(\frac{1}{2} + a_h\right)\int_0^\tau \phi(\tau-\sigma)\left\{\alpha'(\sigma) + \xi''(\sigma) + \left(\frac{1}{2} - a_h\right)\alpha''(\sigma)\right\}\mathrm{d}\sigma + \frac{\pi}{2}a_h(\xi'' - a_h\alpha'') - \left(\frac{1}{2} - a_h\right)\frac{\pi}{2}\alpha' - \frac{\pi}{16}\alpha'' \end{aligned} \tag{4}$$

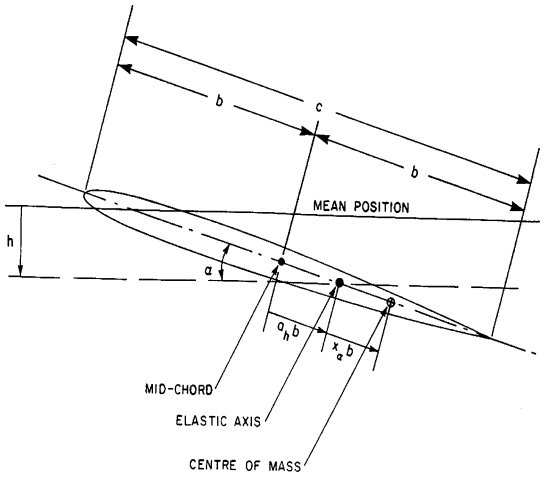

Fig. 1 Schematic of airfoil with two degree-of-freedom motion.

where the Wagner function $\phi(\tau)$ is given by

$$\phi(\tau) = 1 - \psi_1 e^{-\varepsilon_1\tau} - \psi_2 e^{-\varepsilon_2\tau} \tag{5}$$

and the constants $\psi_1 = 0.165$, $\psi_2 = 0.335$, $\varepsilon_1 = 0.0455$, and $\varepsilon_2 = 0.3$ are obtained from Jones.[11] For a cubic spring in the pitch and plunge degrees of freedom, $M(\alpha)$ and $G(\xi)$ in Eqs. (1) and (2) are given by

$$M(\alpha) = \alpha + \beta\alpha^3 \tag{6}$$

$$G(\xi) = \xi + \gamma\xi^3 \tag{7}$$

where β and γ are constants. When $\beta > 0$ and $\gamma > 0$, the pitch and plunge springs are hard, whereas they are called soft springs if $\beta < 0$ and $\gamma < 0$.

Because of the presence of the integral terms in the integrodifferential equations given in Eqs. (1) and (2), it is cumbersome to integrate them numerically. A set of simpler equations was derived by Lee et al.,[3] and they introduced four new variables

$$w_1 = \int_0^\tau e^{-\varepsilon_1(\tau-\sigma)}\alpha(\sigma)\,\mathrm{d}\sigma, \qquad w_2 = \int_0^\tau e^{-\varepsilon_2(\tau-\sigma)}\alpha(\sigma)\,\mathrm{d}\sigma$$

$$w_3 = \int_0^\tau e^{-\varepsilon_1(\tau-\sigma)}\xi(\sigma)\,\mathrm{d}\sigma, \qquad w_4 = \int_0^\tau e^{-\varepsilon_2(\tau-\sigma)}\xi(\sigma)\,\mathrm{d}\sigma \tag{8}$$

The resulting set of eight first-order ordinary differential equations by using Eq. (8) is given as follows:

$$\frac{\mathrm{d}\boldsymbol{X}}{\mathrm{d}\tau} = \boldsymbol{f}(\boldsymbol{X}, \tau) \tag{9}$$

where $\boldsymbol{X} = \{x_1, x_2, \ldots, x_8\} = \{\alpha, \alpha', \xi, \xi', w_1, w_2, w_3, w_4\} \in \boldsymbol{R}^8$. After some algebraic manipulations, the aeroelastic system for a self-excited system with cubic nonlinearities of the form given in Eqs. (6) and (7) can be written as

$$\begin{aligned} &c_0\xi'' + c_1\alpha'' + c_2\xi' + c_3\alpha' + (c_4 + c_{10})\xi + c_5\alpha + c_6 w_1 + c_7 w_2 + c_8 w_3 + c_9 w_4 + c_{10}\gamma\xi^3 = 0 \\ &d_0\xi'' + d_1\alpha'' + d_2\xi' + d_3\alpha' + d_4\xi + (d_5 + d_{10})\alpha + d_6 w_1 + d_7 w_2 + d_8 w_3 + d_9 w_4 + d_{10}\beta\alpha^3 = 0 \\ &w_1' = \alpha - \varepsilon_1 w_1, \qquad w_2' = \alpha - \varepsilon_2 w_2 \\ &w_3' = \xi - \varepsilon_1 w_3, \qquad w_4' = \xi - \varepsilon_2 w_4 \end{aligned} \tag{10}$$

The coefficients c_i and d_i, $i = 0, 1, 2, \ldots, 10$, are functions of system parameters and the expressions are given in the Appendix. Equation (10) can be solved numerically using a fourth-order Runge–Kutta time-marching scheme once the initial conditions $\alpha(0)$, $\alpha'(0)$, $\xi(0)$, and $\xi'(0)$ are specified. The time step in the examples to be given is taken to be $\Delta\tau = 0.1$, which is sufficiently small to produce very accurate results. This value gives a considerably large number of time steps per cycle for a sinusoidal motion recommended by Jones and Lee.[12]

Case Studies

In this paper, the airfoil parameters in the two examples given in Ref. 7 are used to show the effect of coupled nonlinear restoring forces on the airfoil motions. The examples are chosen because they demonstrate the appearance of secondary bifurcations and amplitude-modulated oscillations in primary subcritical Hopf

bifurcations. These are interesting phenomena that have not been observed in previous studies using the same airfoil parameters but with weaker cubic restoring forces. In most studies[3] carried out on the effect of structural nonlinearities on airfoil motion, the damping terms ζ_ξ and ζ_α are set to zero. However, these two terms have a significant influence on the types of airfoil motion in post-Hopf-bifurcation but are often neglected to not introduce extra variables to an already large set of parameters in the study of structural nonlinearities.

Equations (1) and (2) with cubic nonlinearities given by Eqs. (6) and (7) have been studied by Gong et al.[13] for a dynamic system in the absence of the aerodynamic terms. Although including the aerodynamic terms will alter the airfoil motion, this study still gives useful information on the effect of the damping terms. Gong et al.[13] demonstrated mathematically that for $\zeta_\xi > 0$, $\zeta_\alpha > 0$ and $\bar{\omega} > 0$, the equilibrium point (0,0,0,0) is always linearly stable if $x_\alpha < r_\alpha$ and is linearly unstable if $x_\alpha > r_\alpha$. If $\zeta_\xi = \zeta_\alpha = 0$, the point (0,0,0,0) is a nonhyperbolic point and has two pairs of purely imaginary roots when $x_\alpha < r_\alpha$. However, when $x_\alpha > r_\alpha$, the point (0,0,0,0) has a pair of purely imaginary roots plus one positive real root and one negative real root. For airfoil properties that we have studied, x_α is less r_α, and we can conclude from the Gong et al.[13] analysis that when damping terms are included, the motion becomes less complex.

Based on the Gong et al.[13] investigation, we can only generalize that when aerodynamics are included in Eqs. (1) and (2), the effect of damping will have the tendency to make the airfoil motion less complex. Analysis of the stability of the equilibrium point (0,0,0,0) including aerodynamics is too complicated to be carried out mathematically. Another study that also suggests that damping will make the airfoil motion less complex was carried out by Price et al.[14] for a single freeplay in the pitch degree of freedom using Eqs. (1) and (2) with the appropriate expression $M(\alpha)$ for a freeplay. They computed the airfoil motion numerically for four different sets of damping values, that is, $\zeta_\xi = \zeta_\alpha = 0$, $\zeta_\xi = \zeta_\alpha = 0.02$, $\zeta_\xi = \zeta_\alpha = 0.05$, and $\zeta_\xi = \zeta_\alpha = 0.1$. At zero damping, they showed that there is a range of velocity values U^*/U_L^* that indicates chaotic motion. Increasing the damping to 2% of critical value, the bifurcation diagram still shows the same range of velocity where chaotic motion exists. At 5% of the critical value, the chaotic region is reduced, and at 10% of the critical value, the motion becomes periodic. Until further analysis for the cubic nonlinearity has been carried out, we can only assume that the airfoil motion can be more complex when damping is neglected in Eqs. (1) and (2).

Effect of Varying Plunge Stiffness Nonlinearity for Fixed Pitch Nonlinearity

In the first example, the airfoil parameters are: $\mu = 100$, $r_\alpha = 0.5$, $a_h = -0.5$, $\zeta_\xi = \zeta_\alpha = 0$, $x_\alpha = 0.25$, $\bar{\omega} = 0.2$, and $\beta = 80$. With a single nonlinearity in the pitch degree of freedom, $\gamma = 0$, Lee et al.[7] showed that when the freestream velocity reaches the linear flutter velocity $U_L^* = 6.285$, a supercritical Hopf bifurcation occurs. They showed that at $U^*/U_L^* \approx 2$, a secondary subcritical Hopf bifurcation appears and the jump position depends on initial conditions. For example, it varies from $U^*/U_L^* = 1.98$ to $U^*/U_L^* = 2.08$ for $\alpha(0)$ between 0.5 and 10 deg, while keeping $\alpha'(0) = \xi(0) = \xi'(0) = 0$. With different combinations of $\alpha(0)$, $\alpha'(0)$, $\xi(0)$, and $\xi'(0)$, the jump position changes. For the initial conditions they chose, that is, $\alpha(0) = 1$ deg, and $\alpha'(0) = \xi(0) = \xi'(0) = 0$, a small variation in the slope of the pitch amplitude vs the U^*/U_L^* curve is detected at $U^*/U_L^* \approx 2$ for the first harmonic pitch motion. However, there is a large increase in the amplitude of the third harmonic indicating the importance of this harmonic after the jump. For the plunge motion, the jump in the amplitude of the first harmonic is large, whereas that for the third harmonic is small. The third harmonic is significant only in the pitch motion where the nonlinearity is located.

In this paper, with β kept constant at 80, the following values of γ are used: 0.2, 0.5, 0.8, 1.5, 4, 10, 20, and 30. The initial conditions for the time-integration scheme are $\alpha(0) = 1.0$ deg and $\alpha'(0) = \xi'(0) = \xi(0) = 0$. The effects of initial conditions are not considered in this paper because they affect only the jump position in a subcritical Hopf bifurcation, but the basic characteristics of the airfoil response in post-Hopf-bifurcation remain unchanged.

For $\gamma < 0.5$, the primary and secondary bifurcations are similar to those reported in Ref. 7 except for a small increase in the velocity ratio U^*/U_L^* where the secondary bifurcation occurs. In general, the value of U^*/U_L^* at the jump position increases for increasing γ. The amplitudes of the pitch and plunge motions before the jump also increase with γ.

Figure 2a shows the amplitudes of the first and third harmonics pitch motion at $\gamma = 0.5$. The amplitudes are determined from a Fourier analysis of the numerical time series. We note that at $2.18 \le U^*/U_L^* \le 2.28$, there is sharp decrease in the pitch amplitude. Similar to the results given in Ref. 7, the second harmonic is zero, and higher odd harmonics greater than the third are very small. The secondary bifurcation position has now moved to $U^*/U_L^* = 2.28$ instead of $U^*/U_L^* = 1.98$ at $\gamma = 0$. The amplitudes after the primary bifurcation increase by a noticeable amount, for example, the first and third harmonics pitch amplitudes before the sharp drop at $U^*/U_L^* = 2.18$ increase from 9 and 2.2 deg at $\gamma = 0$ to 10.15 and 3.25 deg at $\gamma = 0.5$, respectively.

At $\gamma = 0.5$, the results in Fig. 2b show that the third harmonic plunge amplitude is practically zero because the magnitude of the plunge nonlinearity is not sufficiently large to produce any

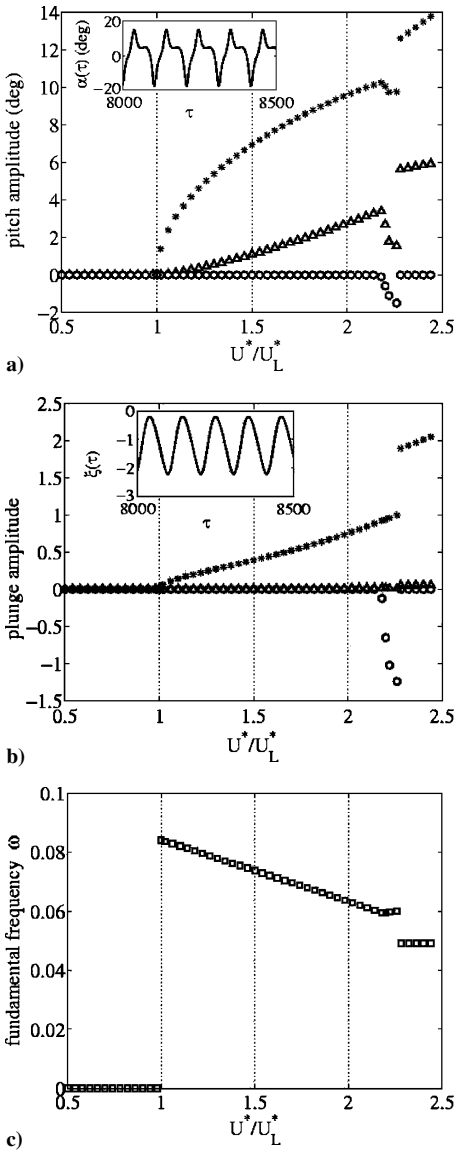

Fig. 2 First and third a) harmonics pitch motion amplitudes and b) harmonics plunge amplitudes; ∗, amplitude of first harmonic; △, amplitude of third harmonic; ○, mean position; and insets in a) and b), time series for $U^*/U_L^* = 2.24$; c) fundamental frequency: $x_\alpha = 0.25$, $\bar{\omega} = 0.2$, $\beta = 80$, and $\gamma = 0.5$.

noticeable third harmonic. However, the first harmonic amplitude increases substantially from $\xi = 0.66$ ($\gamma = 0$) to 0.95 ($\gamma = 0.5$), an increase of nearly 44%. At this value of γ and for motion, for example, just before the jump where the plunge amplitude $\xi = 0.95$, the ratio of the nonlinear to linear stiffness forces in plunge is about 0.4513, which is less than 18% of the value of 2.510 for the ratio in nonlinear/linear restoring pitching moment using an amplitude of 10.15 deg before the jump. Thus, we can see that the plunge nonlinearity, though generating a smaller nonlinear/linear force ratio than the nonlinear/linear moment ratio from the pitch nonlinearity, can have a very noticeable effect on the coupled airfoil motions.

An interesting observation in Figs. 2a and 2b for $2.18 \le U^*/U_L^* \le 2.28$ is the nonzero mean values of the pitch and plunge motions. This is also shown from the time series given in the insets of Figs. 2a and 2b for $U^*/U_L^* = 2.24$. When $U^*/U_L^* > 2.28$, the mean positions return to zero. The mean value is obtained after the transients are discarded and is usually taken in the range $7000 \le \tau \le 9000$, giving, on average, close to 20 cycles of data at the fundamental frequency. Nonzero mean values suggest that a time-averaged lift and a negative pitching moment are acting on the airfoil. This is an interesting phenomenon that suggests that an initial displacement of the airfoil by 1 deg can cause the airfoil to oscillate in a small velocity range with a mean upward vertical displacement and a negative angle of attack. In general, the amplitude jump at the secondary bifurcation point for the plunge motion is about the same for the two values of γ, 1.02 at $\gamma = 0$ vs 0.9 at $\gamma = 0.5$. For the pitch motion, the jumps are 2.9 and 4.2 deg for the first and third harmonics at $U^*/U_L^* = 2.28$ compared to 0 and 3 deg for $\gamma = 0$.

The nondimensional fundamental frequency ω is shown in Fig. 2c. It starts at a value of 0.0835 rad per unit time τ at $U^*/U_L^* = 1$, decreases to 0.058, and remains constant in the range $2.18 \le U^*/U_L^* \le 2.28$. It then jumps to a lower value of 0.048, $\Delta\omega = 0.01$, and remains constant up to $U^*/U_L^* = 2.46$, where the numerical simulations were terminated. The values of ω for $\gamma = 0$ also starts with a value of 0.0835, but the magnitude of the jump is larger, that is, it drops from 0.063 to 0.042, $\Delta\omega = 0.021$.

As the value of γ increases, the amplitude of the airfoil pitch motion also increases. We consider only motions for $\alpha(\tau) \in [-20$ deg, 20 deg]. The aerodynamics given by Fung[10] is for a thin airfoil based on the assumption of attached flow. The extreme values of $\alpha(\tau) = \pm 20$ deg exceed the limiting value at which the aerodynamics becomes invalid by a substantial amount (at least 5–10 deg depending on flow velocity). Some results are given up to this value of $\alpha(\tau)$ for the purpose of showing the trends only. However, they should be interpreted with caution when comparing to experiments because any flow separations will invalidate the unsteady aerodynamics used in the analysis. From the numerical simulations, it is found that the velocity ratio satisfying the attached flow assumption decreases with increasing γ; for example, at $\gamma = 0.5$, the computations terminate at $U^*/U_L^* = 2.46$, whereas for the next value of γ investigated, $\gamma = 0.8$, the computations should not be continued beyond $U^*/U_L^* = 2.3$. We note that at this value of γ, the mean pitch amplitude is positive whereas the plunge amplitude is still negative. This implies a reversal in the static pitching moment to a positive value while the lift is still in the upward direction. The sharp change in mean amplitude has moved forward to $U^*/U_L^* = 2.06$. The mean pitch and plunge positions have not returned to zero, even when the computations are continued to $U^*/U_L^* = 2.5$.

At $\gamma = 1.5$ and higher up to the largest value studied, $\gamma = 30$, the pitch motions for values of the velocity ratio up to $U^*/U_L^* \approx 2.2$ are approximately within the range $\alpha(\tau) \in [-20$ deg, 20 deg]. In the range $0.8 \le \gamma \le 4$, a jump in the pitch/plunge amplitudes is not observed, but instead a rapid drop followed by more gradual rise in amplitude is detected for the pitch first and third harmonics, whereas the plunge third harmonic is practically zero, and the change in the first harmonic is hardly noticeable in the range of U^*/U_L^* where rapid pitch motion changes are detected. The mean values for both pitch and plunge motions retain nonzero values up to $U^*/U_L^* = 2.2$, where the computations are terminated. Typically, the region of rapid changes is small, of the order of $\Delta U^*/U_L^* = 0.1$. The frequency does not exhibit sharp or large changes at the value of $U^*/U_L^* \approx 2$ for $\gamma = 1.5$ and ≈ 1.9 for $\gamma = 4$, where the rapid changes in pitch/plunge amplitudes are observed.

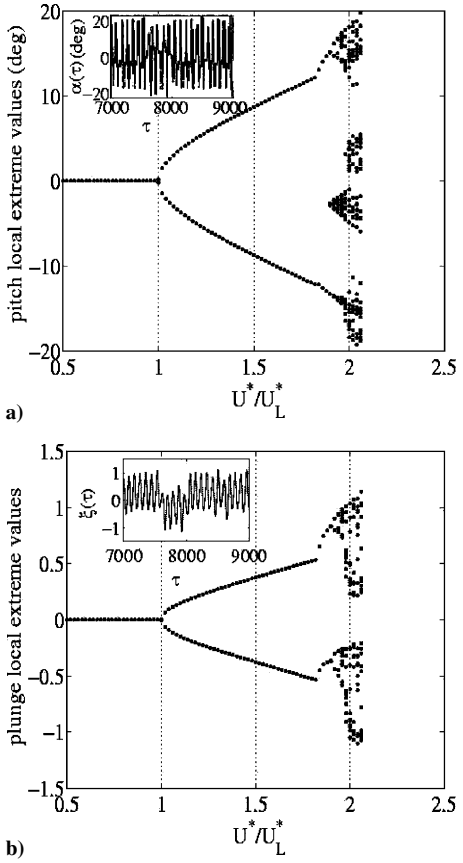

Fig. 3 Bifurcation diagrams for $x_\alpha = 0.25$, $\bar{\omega} = 0.2$, $\beta = 80$, and $\gamma = 10$: a) pitch motion and b) plunge motion; insets, time series for $U^*/U_L^* = 2.05$.

A different behavior pattern emerges at $\gamma = 10$. The local extreme values (maximum or minimum) of the pitch/plunge motions evaluated at $\alpha'(\tau) = 0$ and $\xi'(\tau) = 0$, respectively, are shown in Figs. 3a and 3b. The local extreme value increases smoothly up to $U^*/U_L^* = 1.8$, and Figs. 3a and 3b show a more rapid increase for $1.8 \le U^*/U_L^* \le 1.9$. In the range $1.9 \le U^*/U_L^* \le 2.06$, a large number of peaks in the time series are detected. The numerical time integration stops at $\tau = 9000$, which is sufficiently long for the cases so far investigated in this section. The airfoil motion in this small range of U^*/U_L^* appears to be chaotic. The time series at $U^*/U_L^* = 2.05$ are shown in the insets of Fig. 3. A power spectral density plot is shown in Fig. 4a. The results are very similar to those given by Price et al.,[15] who showed that this type of power spectral density is indicative of chaos in an aeroelastic system with concentrated structural nonlinearities. Furthermore, they evaluated the Lyapunov exponents and found that one exponent was positive, thus, giving further evidence of the existence of chaos. The Poincaré section shown in Fig. 4b has a very distinct structure that lends further evidence to the existence of chaotic motions. It may be beneficial to carry out the numerical integration to longer times to ensure that the behavior is truly independent of the time duration in the simulation, but a closer study of the time series suggest that the results will probably not alter the conclusions drawn from the existing computations.

For the next value of $\gamma > 10$ investigated, the bifurcation behavior of the pitch/plunge motions reverts back to those similar for small values of $\gamma < 0.5$. The mean values of the pitch and plunge motions become zero, and abrupt changes in the amplitudes and frequency occur in which the motions jump directly from one-peak to three-peak motions. Figure 5a shows a bifurcation diagram of the pitch motion for $\gamma = 20$, in which the amplitude jumps at $U^*/U_L^* = 1.74$. Unlike the case for $\gamma = 0$ in Ref. 7, the amplitude of the first

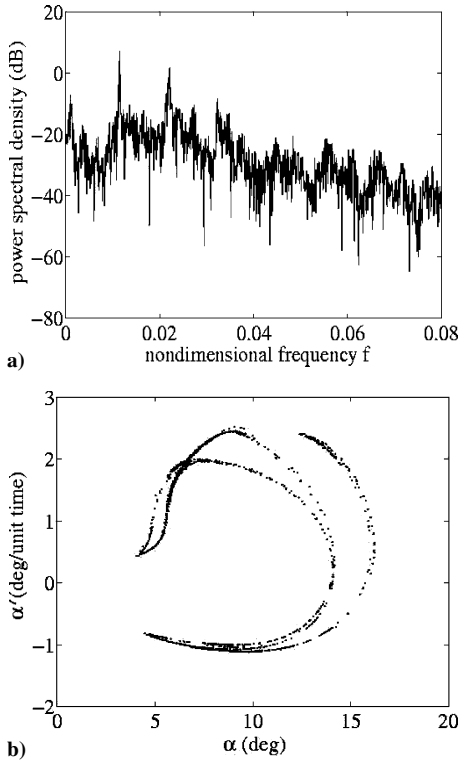

Fig. 4 Pitch motion for $x_\alpha = 0.25$, $\bar{\omega}$=0.2, $\beta = 80$, $\gamma = 10$, and $U^*/U_L^* = 2.05$: a) power spectral density plot and b) Poincaré section, for $\xi' = 0$ and $\xi > 0$.

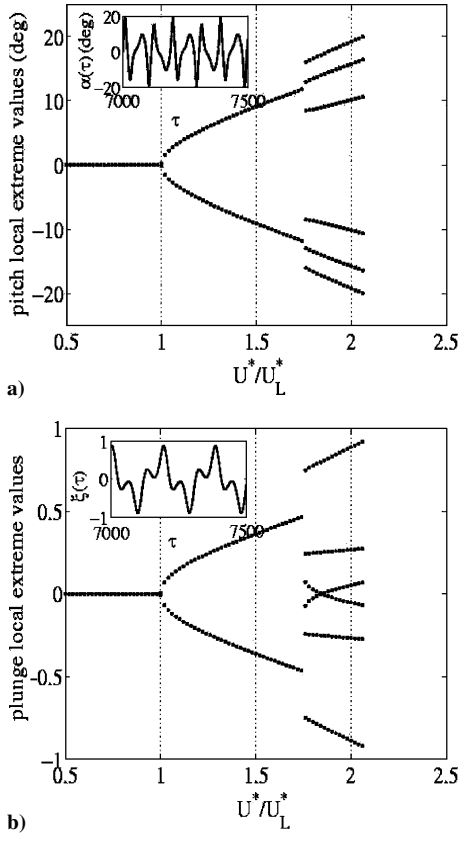

Fig. 5 Bifurcation diagrams for $x_\alpha = 0.25$, $\bar{\omega} = 0.2$, $\beta = 80$, and $\gamma = 20$: a) pitch motion and b) plunge motion; insets, time series for $U^*/U_L^* = 2$.

harmonic decreases dramatically, whereas the amplitude of the third harmonic increases sharply for the motion after the jump. For example, at the bifurcation point, the first harmonic pitch amplitude decreases from 10 to 2 deg, whereas the third harmonic increases from 1.6 to 7.8 deg. Beyond the bifurcation point, the amplitude of the third harmonic grows slightly faster than that of the first harmonic. Thus, the third harmonic is the more dominant term in the Fourier representation of the time series in postsecondary Hopf bifurcation for this value of γ. The plunge motion bifurcation diagram is shown in Fig. 5b. Similar to the pitch degree of freedom, the plunge motions also exhibit a jump from one-peak to three-peak behavior. At $U^*/U_L^* = 1.74$, the first harmonic plunge amplitude decreases from $\xi = 0.46$ to 0.35, and the third harmonic increases from $\xi = 0$ to 0.34. The increase in amplitude of the first harmonic for $U^*/U_L^* > 1.74$ is more rapid than that of the third, and, hence, it is still the dominant Fourier component in the plunge motion. Shown in the insets of Fig. 5 are time series for$U^*/U_L^* = 2$, and we can clearly see the presence of the third harmonic.

For the last case considered in this study where $\gamma = 30$, the results are very similar to those for $\gamma = 20$.

In the example described in this section, where β is fixed and γ varies, we demonstrate that by varying the magnitude of the nonlinear/linear restoring forces in the plunge degree of freedom, the motion can change quite significantly, switching from one type to another abruptly. There are ranges of γ where a secondary bifurcation occurs, and a narrow window of γ where chaotic motions are possible.

Effect of Varying Pitch Stiffness Nonlinearity for Fixed Plunge Nonlinearity

Ideally, it would be informative to repeat the numerical study just described by choosing different values of β and varying γ for each fixed β. This would then be followed by similar studies with γ fixed and β varying, repeating for various values of γ. The test matrix for such a study will be extremely huge and require a large amount of computations. Deducing any behavior pattern would become quite difficult, if not impractical, using numerical simulations. An analytical approach will help to predict trends, but unfortunately this requires a higher harmonic balance method[8] that requires as much, if not greater, computational effort. We did not carry out such a detailed study, but instead performed some limited investigations on two cases based on the second example given in Ref. 7.

Lee et al.[7] investigated the effect of natural frequency ratio $\bar{\omega}$ on the bifurcation of a two-dimensional airfoil motion with $\gamma = 0$ and $\beta = 80$. Three values of $\bar{\omega} = 1$, 1.2, and 1.4 were studied, with most of the airfoil parameters the same as those given in the preceding subsection, except that $x_\alpha = 0.1$. The more interesting case is for $\bar{\omega} = 1.2$, where it is shown that the primary bifurcation is a subcritical Hopf bifurcation. On the upper branch of the bifurcation curve, there is a segment in the range $0.9643 \le U^*/U_L^* \le 1.1508$ where the solution is unstable. The numerical computations show the pitch/plunge motions to be amplitude modulated. When the perturbation-incremental method[9] is used, it can be shown from Ref. 7 that, within this range of U^*/U_L^*, a torus bifurcation occurs in which a pair of Floquet multipliers crosses the unit circle at points other than ± 1, and the stable solutions are tori. Limit-cycle oscillations become stable again for $U^*/U_L^* > 1.1508$.

In this paper, we investigate effect of the coupled pitch/plunge nonlinearities by considering $\bar{\omega} = 1.2$ and keeping the plunge nonlinearity fixed at $\gamma = 10$. The values of β investigated are 0, 0.1, 0.5, 5, 10, 15, 20, 30, 50, and 80. The initial conditions in the time-marching scheme are the same as the preceding section, that is, $\alpha(0) = 1.0$ deg, $\alpha'(0) = \xi'(0) = \xi(0) = 0$.

The reference case for $\beta = 0$, $\gamma = 10$ is shown in Fig. 6, where the pitch/plunge amplitudes and the fundamental frequency are shown. The pitch/plunge amplitudes show that the first harmonic is dominant and the third harmonic increases very slowly with U^*/U_L^*. At a value of $U^*/U_L^* = 4$, α and ξ are approximately 0.5 deg and 0.02, respectively. When a value of $\xi = 0.52$ is taken at this value of U^*/U_L^*, the nonlinear/linear plunge force ratio is about 2.7. The results

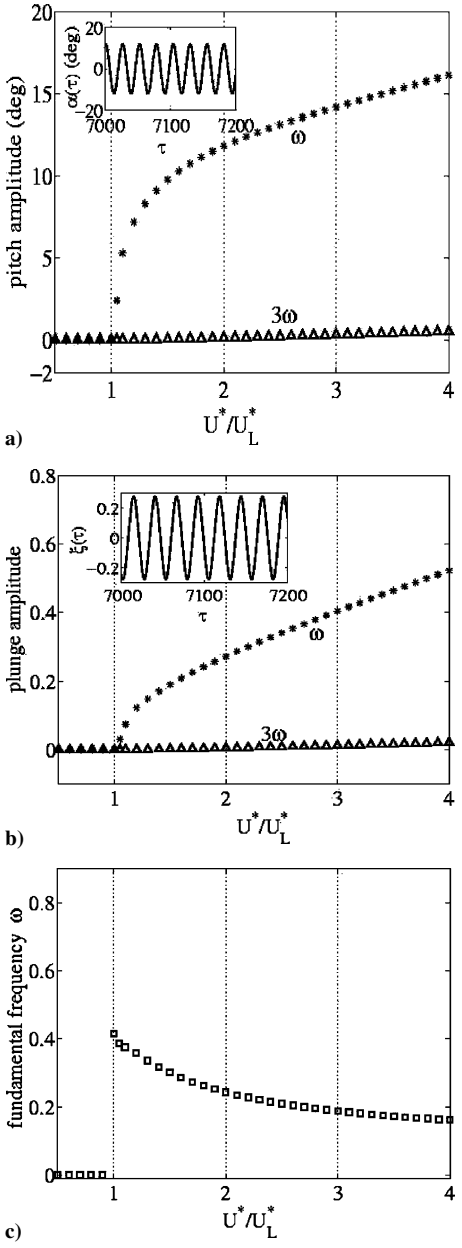

Fig. 6 First and third a) harmonics pitch motion amplitudes and b) harmonics plunge motion amplitudes; c) fundamental frequency: $x_\alpha = 0.1$, $\bar{\omega} = 1.2$, $\beta = 0$, and $\gamma = 10$. $*$, amplitude of first harmonic and $\triangle$, amplitude of third harmonic; insets, the time series for $U^*/U_L^* = 2$.

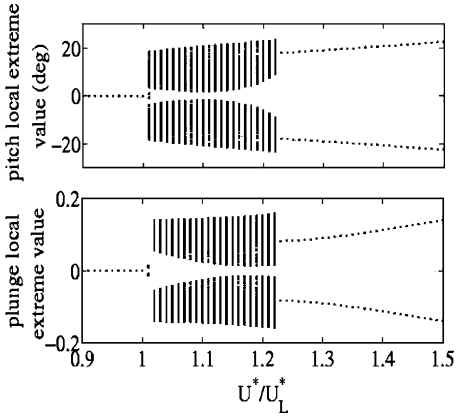

Fig. 7 Pitch and plunge bifurcation diagrams for $x_\alpha = 0.1$, $\bar{\omega} = 1.2$, $\beta = 10$, and $\gamma = 10$.

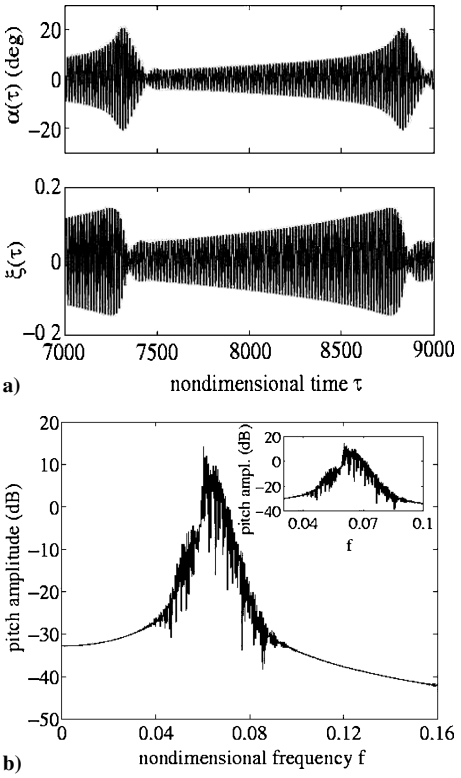

Fig. 8 Pitch and plunge motions: $x_\alpha = 0.1$, $\bar{\omega} = 1.2$, $\beta = 10$, $\gamma = 10$, and $U^*/U_L^* = 1.1$.

indicate that a larger value of γ is necessary to produce a larger third harmonic. The time series of the motions in the insets of Figs. 6 computed at $U^*/U_L^* = 2$ clearly show a sinusoidal behavior. The bifurcation is of the supercritical type at a value $U^* = U_L^* = 2.951$. No secondary bifurcation is observed up to a value of $U^*/U_L^* = 4$, where the computations were terminated. The value of the plunge nonlinearity is not very large compared to the later pitch nonlinearity. For this case, at a value of $U^*/U_L^* = 2.5$, $\xi = 0.35$ and the ratio of the plunge nonlinear/linear restoring forces is 1.225.

Up to $\beta = 5$, a supercritical Hopf bifurcation is observed at $U^*/U_L^* = 1$, and a small increase in the amplitudes of the pitch/plunge motions is observed. When β reaches a value of 10, the bifurcation switches to the subcritical type (Fig. 7) and the pitch/plunge time series show that between $1.01 \le U^*/U_L^* \le 1.22$ the motions are amplitude modulated. These limits are accurate up to $\Delta U^*/U_L^* = 0.01$, which is the increment of U^*/U_L^* used in the numerical simulations. Typical time series of the pitch and plunge motions at $U^*/U_L^* = 1.1$ are shown in Fig. 8a, where approximately one cycle of the modulated motions is shown. Some of the peak pitch amplitudes in Fig. 8a are very close to the limit $\alpha(\tau) \in [-20 \text{ deg}, 20 \text{ deg}]$ that we impose on the validity of the aerodynamics. The modulation frequency f_m computed from Fig. 8a is approximately 0.0007. The fast Fourier transform (FFT) plot of the pitch motion shown in Fig. 8b shows a broadband peak at a frequency $f \approx 0.06$, and the bandwidth of the peak is approximately $\Delta f = 0.03$. The inset in Fig. 8b shows an enlarged portion of the FFT plot in the range $0.04 \le f \le 0.1$. No particular structure can be deduced from Fig. 8b. However, an FFT computed at different U^*/U_L^* shows a structure in the frequency contents of the peak . For example, at $U^*/U_L^* = 1.2$, the broad peak of Fig. 9 shows a number of sharp finer peaks similar to that observed in Ref. 7. The frequency separation Δf between adjacent peaks is fairly constant and is approximately 0.002. Some of the values of the finer peaks are given in Fig. 9. Although an explanation of the modulation was not given in Ref. 7, Lee et al.[7] pointed out that the modulation frequency was the same as the frequency separation Δf within computational errors, leading us to attribute the modulation to being the result of interaction between the different frequencies.

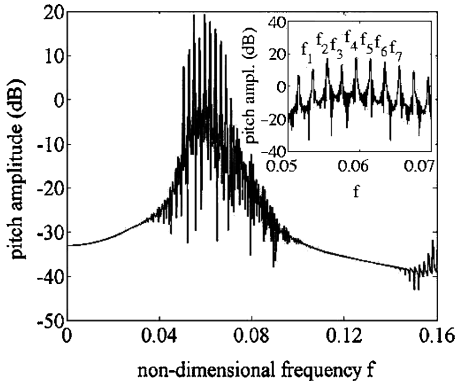

Fig. 9 Pitch amplitude for $x_\alpha = 0.1$, $\bar{\omega} = 1.2$, $\beta = 10$, $\gamma = 10$, and $U^*/U_L^* = 1.2$: $f_1 = 0.0535$, $f_2 = 0.0554$, $f_3 = 0.0575$, $f_4 = 0.0594$, $f_5 = 0.0615$, $f_6 = 0.0635$, and $f_7 = 0.0655$.

When β is increased from 10 to 80, the pitch/plunge amplitudes decrease and the range of U^*/U_L^* where the oscillations are amplitude modulated decreases. The modulation frequency increases with β. For example, for $U^*/U_L^* = 1.1$, we computed f_m as follows: at $\beta = 10$, $f_m = 0.0007$; at $\beta = 15$, $f_m = 0.0012$; at $\beta = 20$, $f_m = 0.0016$; at $\beta = 30$, $f_m = 0.0019$; at $\beta = 50$, $f_m = 0.0021$; and at $\beta = 80$, $f_m = 0.0023$. Also, f_m changes with U^*/U_L^*. For example, at $\beta = 10$ and $U^*/U_L^* = 1.2$, $f_m = 0.002$ instead of 0.0007 at $U^*/U_L^* = 1.1$. There are not sufficient data for other values of U^*/U_L^* to show the trend in the variation of f_m with β.

To obtain an estimate of the effect of $\bar{\omega}$, we performed some computations where ω_ξ is 20% smaller instead of 20% larger than ω_α, that is, $\bar{\omega} = 0.8$. In this case, γ is kept constant at 30 and the values of β used are 0, 0.5, 2, 5, 10, 15, 20, 30, 50, and 80. At the two smallest values of $\beta = 0$ and 0.5, a subcritical Hopf bifurcation occurs at $U^*/U_L^* = 1$. At $\beta = 2$, the time series shows a modulated wave similar to that shown in Fig. 7 for $\bar{\omega} = 1.2$, $\beta = 10$, and $\gamma = 10$. However, this phenomenon occurs only in a very narrow range of U^*/U_L^*. The amplitude can go as high as 40 deg close to the bifurcation point and exceeds our requirement that $\alpha(\tau) \in [-20 \text{ deg}, 20 \text{ deg}]$ for the flow to be attached and for the aerodynamics given by Fung[8] to be valid. At $\beta = 5$, the primary bifurcation at $U^*/U_L^* = 1$ switches to the supercritical type, and the pitch/plunge amplitudes increase rapidly such that the condition $\alpha(\tau) \in [-20 \text{ deg}, 20 \text{ deg}]$ cannot be satisfied for $U^*/U_L^* > 1.1$. The bifurcation remains supercritical for increasing β, and the pitch/plunge amplitudes increase at a slower rate, thus increasing the range of U^*/U_L^* where the numerical simulation can be conducted. For example, at $\beta = 10$, the condition $\alpha(\tau) \in [-20 \text{ deg}, 20 \text{ deg}]$ holds at $U^*/U_L^* \leq 1.3$, and this value increases with β. The modulated wave phenomenon disappears at $\beta = 50$, even when the computations are carried out up to $U^*/U_L^* \leq 3$ when the pitch amplitude reaches the maximum limit we impose at 20 deg. Up to the largest value studied, $\beta = 80$, a secondary bifurcation as observed for $\bar{\omega} = 0.2$ described in the preceding subsection, where a supercritical Hopf bifurcation changes to a subcrtitical bifurcation, is not detected up to a value of $U^*/U_L^* = 3.5$, where the maximum pitch amplitude reaches a value of 30 deg, rendering the aerodynamics invalid. A case with $\beta = 80$ and $\gamma = 0$ is carried out for comparison purposes. Results available at the highest value computed for this case, $U^*/U_L^* = 1.5$, when compared with those for $\beta = 80$ and $\gamma = 30$, show that γ has a greater effect on the pitch amplitude, which increases from 4.5 ($\gamma = 0$) to 6 deg ($\gamma = 30$), whereas the plunge amplitude varies from 0.12 ($\gamma = 0$) to 0.13 ($\gamma = 30$), which is effectively unchanged.

The example described in this section shows that for a fixed value of γ ($\gamma = 30$ in this case), the value of β determines the type of primary bifurcation. Also, for small values of β where the bifurcation is subcritical, small increases in β causes large increases in pitch/plunge amplitudes. Once the value β is reached when the bifurcation switches to supercritical, the amplitudes decrease with increasing β.

Conclusions

The complexity of the aeroelastic equations of motion of an airfoil with coupled nonlinear restoring forces makes it impractical to derive analytical methods to predict bifurcation behavior. The commonly used harmonic balance method for nonlinear problems can be extended to give fairly accurate results in some special cases. In general, a large number of terms have to be included in the Fourier series representation, and a frequency–amplitude relation cannot be derived analytically. A trend or parametric study requires a large amount of computations because of the numerous combinations of airfoil parameters and spring constants that generate the nonlinear restoring forces. In addition, it is often not possible to predict from extrapolation the sudden change in response characteristics when the bifurcation parameter is varied. For this reason, only a case-by-case study is the normal approach. From numerical simulations, it is shown that coupled nonlinearities can generate a variety of interesting response phenomena, such as primary and secondary Hopf bifurcations and modulated oscillations in subcritical Hopf bifurcations. Chaotic behavior is possible in a narrow window of the bifurcation parameter. When a value of the frequency parameter $\bar{\omega} = 0.2$ is used, it is shown that for a fixed pitch cubic nonlinearity of fairly large value ($\beta = 80$), the value of U^*/U_L^* at the jump position where secondary bifurcation occurs increases for increasing γ. The third harmonic for the pitch motion is usually small. Also, in some cases nonzero mean values of the pitch and plunge motions are observed. At sufficient large value of γ ($\gamma = 10$), chaotic motion is detected. With a further increase in γ, the bifurcation behavior reverts back to that for small values of $\gamma < 0.5$. When a larger value of $\bar{\omega} = 1.2$ is used and γ is kept at 10, a supercritical Hopf bifurcation is observed at $U^*/U_L^* = 1$ for $\beta \leq 5$. For larger values of β, a subcritical Hopf bifurcation occurs. The pitch/plunge motions are amplitude modulated, and the spectra show a large number of discrete frequency peaks. The separation frequency is approximately constant and equal to the modulation frequency.

Appendix: Coefficients in Aeroelastic Equations [Eq. (11)]

$$c_0 = 1 + 1/\mu, \qquad c_1 = x_\alpha - a_h/\mu$$

$$c_2 = 2(1 - \psi_1 - \psi_2)/\mu + 2\zeta_\xi \bar{\omega}/U^*$$

$$c_3 = [1 + (1 - 2a_h)(1 - \psi_1 - \psi_2)]/\mu$$

$$c_4 = 2(\varepsilon_1\psi_1 + \varepsilon_2\psi_2)/\mu$$

$$c_5 = 2\left[1 - \psi_1 - \psi_2 + \left(\tfrac{1}{2} - a_h\right)(\varepsilon_1\psi_1 + \varepsilon_2\psi_2)\right]\Big/\mu$$

$$c_6 = 2\varepsilon_1\psi_1\left[1 - \varepsilon_1\left(\tfrac{1}{2} - a_h\right)\right]\Big/\mu$$

$$c_7 = 2\varepsilon_2\psi_2\left[1 - \varepsilon_2\left(\tfrac{1}{2} - a_h\right)\right]\Big/\mu, \qquad c_8 = -2\varepsilon_1^2\psi_1\Big/\mu$$

$$c_9 = -2\varepsilon_2^2\psi_2\Big/\mu, \qquad c_{10} = (\bar{\omega}/U^*)^2, \qquad d_0 = x_\alpha\Big/r_\alpha^2 - a_h\Big/\mu r_\alpha^2$$

$$d_1 = 1 + \left(1 + 8a_h^2\right)\Big/8\mu r_\alpha^2$$

$$d_2 = -(1 + 2a_h)(1 - \psi_1 - \psi_2)\Big/\mu r_\alpha^2$$

$$d_3 = (1 - 2a_h)\Big/2\mu r_\alpha^2 - (1 + 2a_h)(1 - 2a_h)(1 - \psi_1 - \psi_2)\Big/2\mu r_\alpha^2 + 2\zeta_\alpha/U^*$$

$$d_4 = -(1 + 2a_h)(\varepsilon_1\psi_1 + \varepsilon_2\psi_2)\Big/\mu r_\alpha^2$$

$$d_5 = -(1 + 2a_h)(1 - \psi_1 - \psi_2)\Big/\mu r_\alpha^2 - (1 + 2a_h)(1 - 2a_h)(\psi_1\varepsilon_1 - \psi_2\varepsilon_2)\Big/2\mu r_\alpha^2$$

$$d_6 = -(1 + 2a_h)\psi_1\varepsilon_1\left[1 - \varepsilon_1\left(\tfrac{1}{2} - a_h\right)\right]\Big/\mu r_\alpha^2$$

$$d_7 = -(1 + 2a_h)\psi_2\varepsilon_2\left[1 - \varepsilon_2\left(\tfrac{1}{2} - a_h\right)\right]\Big/\mu r_\alpha^2$$

$$d_8 = (1 + 2a_h)\psi_1\varepsilon_1^2\Big/\mu r_\alpha^2, \qquad d_9 = (1 + 2a_h)\psi_2\varepsilon_2^2\Big/\mu r_\alpha^2$$

$$d_{10} = (1/U^*)^2$$

References

[1]Woolston, D. S., Runyan, H. L., and Andrews, R. E., "An Investigation of Effects of Certain Types of Structural Nonlinearities on Wing and Control Surface Flutter," *Journal of the Aeronautical Sciences,* Vol. 24, No. 1, 1957, pp. 57–63.

[2]Shen, S. F., "An Approximate Analysis of Nonlinear Flutter Problems," *Journal of the Aeronautical Sciences,* Vol. 26, No. 1, 1959, pp. 25–32.

[3]Lee, B. H. K., Price, S. J., and Wong, Y. S., "Nonlinear Aeroelastic Analysis of Airfoils: Bifurcation and Chaos," *Progress in Aerospace Sciences,* Vol. 35, No. 3, 1999, pp. 205–334.

[4]O'Neil, T., and Strganac, T. W., "Aeroelastic Response of a Rigid Wing Supported by Nonlinear Springs," *Journal of Aircraft*, Vol. 35, No. 4, 1998, pp. 616–622.

[5]Hauenstein, A. J., Zara, J. A., Eversman, W., and Qumei, I. K., "Chaotic and Nonlinear Dynamic Response of Aerosurfaces with Structural Nonlinearities," *Proceedings of the 33rd AIAA/ASME/ASCE/AHS/ASC Structures, Structural Dynamics, and Materials Conference*, AIAA-92-2547 CP, AIAA, Washington, DC, 1992, pp. 2367–2375.

[6]Alighanbari, H., "Flutter Analysis and Chaotic Response of an Airfoil Accounting for Structural Nonlinearities," Ph.D. Dissertation, Dept. of Mechanical Engineering, McGill Univ., Montreal, 1995.

[7]Lee, B. H. K., Liu, L., and Chung, K. W., "Airfoil Motion in Subsonic Flow with Strong Cubic Nonlinear Restoring Forces," *Journal of Sound and Vibration*, Vol. 281, No. 3–5, 2003, pp. 699–717.

[8]Liu, L., and Dowell, E. H., "The Secondary Bifurcation of an Aeroelastic Airfoil Motion: Effects of Higher Harmonics," *Nonlinear Dynamics*, Vol. 37, No. 1, 2004, pp. 31–49.

[9]Chung, K. W., Chan, C. L., Xu, Z., and Mahmoud, G. M., "A Perturbation-Incremental Method for Strongly Nonlinear Oscillators with Many Degrees of Freedom," *Nonlinear Dynamics*, Vol. 28, No. 3–4, 2002, pp. 243–259.

[10]Fung, Y. C., *An Introduction to the Theory of Aeroelasticity*, Dover, New York, 1993, p. 212.

[11]Jones, R. T., "The Unsteady Lift of a Wing of Finite Aspect Ratio," NACA Rept. 681, Jan. 1940.

[12]Jones, D. J., and Lee, B. H. K., "Time Marching Numerical Solution of the Dynamic Response of Nonlinear Systems," National Research Council, Rept. NAE-AN-25, Ottawa, Jan. 1985.

[13]Gong, L., Wong, Y. S., and Lee, B. H. K., "Dynamics of a Coupled System of Duffing's Equations," *Dynamics of Continuous, Discrete and Impulsive Systems*, Vol. 4, No. 1, 1998, pp. 99–119.

[14]Price, S. J., Alighanbari, H., and Lee, B. H. K., "The Aeroelastic Response of a Two-Dimensional Airfoil with Bilinear and Cubic Structural Nonlinearities," *Journal of Fluids and Structures*, Vol. 9, No. 2, 1995, pp. 175–193.

[15]Price, S. J., Lee, B. H. K., and Alighanbari, H., "Postinstability Behavior of a Two-dimesnional Airfoil with a Structural Nonlinearity," *Journal of Aircraft*, Vol. 31, No. 6, 1994, pp. 1395–1401.